

Primljen / Received: 25.10.2023.

Ispravljen / Corrected: 15.3.2024.

Prihvaćen / Accepted: 28.3.2024.

Dostupno online / Available online: 10.5.2024.

Fracture performance of externally FRP strengthened reinforced concrete beams mixed with rigid fibres

Authors:

Original research paper



Assoc. Prof. **Syed Muhammad Syed Ibrahim**, PhD. CE
Ilahia College of Engineering and Technology, India
Department of Civil Engineering
syed_ibms@yahoo.co.in
Corresponding author



Prof. **Selvaraj Kandasamy**, PhD. CE
Vel Tech Rangarajan Dr. Sagunthala R&D Institute
of Science and Technology, India
Department of Civil Engineering
drskandasamy@veltech.edu.in



Assist. Prof. **Jagadeesan Thivya**, PhD. CE
University College of Engineering Dindigul, India
Department of Civil Engineering
thivyame@gmail.com



Assist. Prof. **Jagadeesan Vijayaraghavan**, PhD. CE
University College of Engineering
Ramanathapuram, India
Department of Civil Engineering
drjvr1988@gmail.com

Syed Muhammad Syed Ibrahim, Selvaraj Kandasamy, Jagadeesan Thivya, Jagadeesan Vijayaraghavan Fracture performance of externally FRP strengthened reinforced concrete beams mixed with rigid fibres

In recent decades experimental investigations on fibre reinforced polymer (FRP) laminate-strengthened reinforced concrete (RC) beams have been extensively conducted. It has been found effective in flexural and shear strengthening perspectives. On the other hand, a primary problem frequently encountered in such technique is the separation of FRP laminate with the concrete bonded surface. Such failures are due to the formation of localized flexural and otherwise shear cracks in the fragile region of the FRP-concrete interface. The debonding occurrence also significantly affects the strength enhancement of the laminated beams. The emphasis of the study is to enhance the potential performance of externally FRP strengthened RC beams by incorporating an effective crack controlling agent, that is 'rigid hooked-end steel fibres' in the matrix. Nine RC beams were cast and tested in this study with variables including different quantities of hooked-ends steel and glass fibre reinforced polymer (GFRP) thickness. The pre-cracking and post-cracking behaviour of the externally FRP strengthened RC beams mixed with the short fibres were systematically evaluated and improved performance at various stages of cracking was found. Another finding is the transformation of failure pattern from brittle to ductile due to exceptional strain-hardening phenomenon caused by steel fibres in the strengthened RC beams, in comparison to that of other beams without steel fibres. The formations and propagations of the cracks at different stages were numerically modelled for all the beams using the ANSYS and compared the numerical design validation with the experiment.

Key words:

reinforced concrete beams, SFRC, GFRP, steel fibre, debonding, crack-width, FEA, ANSYS

Izvorni znanstveni rad

Syed Muhammad Syed Ibrahim, Selvaraj Kandasamy, Jagadeesan Thivya, Jagadeesan Vijayaraghavan Ponašanje tijekom sloma izvana pojačanih armiranobetonskih greda s primjesom krutih vlakana

Posljednjih desetljeća opsežno su provedena eksperimentalna istraživanja na armiranobetonskim (AB) gredama pojačanim vlaknima. Utvrđena je učinkovitost u području pojačanja na savijanje i posmik. S druge strane, primarni problem koji se često susreće u takvoj tehnici jest odvajanje FRP laminata od betonske površine. Takva otkazivanja nastaju zbog formiranja lokaliziranih savojnih i posmičnih pukotina u krhkom području FRP betona. Pojava odvajanja također značajno utječe na povećanje nosivosti pojačanih greda. Težište istraživanja je poboljšati potencijalno ponašanje izvana pojačanih AB greda FRP-om dodavanjem učinkovitog sredstva za kontrolu pukotina u matricu, a to su "kruta čelična vlakna s kukastim krajevima". Izvedeno je devet AB greda i ispitano u ovom istraživanju s varijablama uključujući različite količine čeličnih vlakana s kukastim krajevima i debljinu polimera armiranih staklenim vlaknima. Ponašanje izvana FRP-om pojačanih AB greda pomiješanih s kratkim vlaknima prije i nakon raspucavanja sustavno je procijenjeno i utvrđeno je poboljšano djelovanje u različitim fazama raspucavanja. Drugo otkriće je transformacija oblika loma iz krtog u duktilni zbog izuzetnog fenomena deformacijskog očvršćivanja uzrokovanog čeličnim vlaknima u pojačanim AB gredama, u usporedbi s ostalim gredama bez čeličnih vlakana. Formiranje i širenje pukotina u različitim fazama numerički je modelirano za sve grede uporabom ANSYS-a i uspoređena je validacija numeričkog modela s eksperimentom.

Ključne riječi:

armiranobetonske grede, SFRC, GFRP, čelična vlakna, odvajanje, širina pukotine, FEA, ANSYS

1. Introduction

“Structural strengthening” is a method of improving the load-carrying capacity against an existing condition of the structures. There are several advantages of structural strengthening, such as (i) increasing the load-carrying capacity and stiffness in the least construction time with minimal or no disruption to traffic or other operation(s), (ii) being cost-effective as it avoids removal and reconstruction, and (iii) reducing the materials wastage and consequently reducing environmental degradation to some extent. Strengthening by external fibre reinforced polymer (FRP) bonding or lamination method has been found superior to other methods because of its several proven advantages in various aspects, such as strength (i.e., high strength-to-weight ratio and high fatigue strength), stiffness (i.e., high stiffness-to-weight ratio), and durability in most adverse environments, non-magnetic and non-conductive properties, and a great extent of chemical inertness [1-7].

In past decades the experimental investigations pertaining to externally FRP laminated reinforced concrete (RC) beams under static loading have been extensively carried out [8-11]. So far, seven different failure modes have been determined and reported in the literature in respect of the above FRP plate-bonding technique. They are: (a) Shear failure, (b) Rupture failure, (c) Concrete crushing failure, (d) Cover failure, (e) FRP end interfacial debonding failure, (f) Interfacial flexural-shear induced debonding failure, and (g) Interfacial flexural crack induced debonding failure. Of the above, types (d) to (g) all show premature debonding failures, and such modes of failures significantly limit the performance of FRP strengthened beams [12-14]. The reason reported in most of their studies remains premature debonding of FRP, which starts because of the formation of localized flexural cracks in the weaker tension zone of the concrete element. On further loading, the cracks consistently propagate and widen (i.e., increase in crack-width) within the fracture mode and towards the threshold of the

FRP-concrete interface, which seriously disturbed the bonding phenomenon of adhesive resin [15-17].

Control on the formation of such localized cracks can be made possible by adding randomly oriented short, discrete fibres into a fresh-state of concrete [18-21]. Hence, this study intended to control the formation of cracks on externally bonded FRP strengthened RC beams by adding a crack-controlling agent, “3D hooked-end steel fibres”, into the concrete matrix. The primary objectives of incorporating fibres into concrete are to enhance the tensile and toughness properties, resulting in increased cracking and deformation characteristics of hardened concrete [22-25]. The study parameters include crack-widths at various (first-crack, yield and ultimate) stages, crack formation, crack spacing, and failure pattern of the test beams. The beams consisted of different proportions of discrete hooked-end steel fibres (0 %, 0.5 %, 1 %, and 1.5 %) and were then externally bonded by two different thicknesses (3 and 5 mm) of glass fibre reinforced polymer (GFRP) laminates. All the beams were indulged in the same environment of static monotonic loading. The beam results were evaluated systematically and discussed, while also comparing the above results with and without FRP strengthened RC beams.

2. Experimental work

2.1. Characterization of materials

Conventional materials such as Portland pozzolana cement (PPC), nearby existing river sand (as fine aggregate), and 20 mm well-graded crushed granite (as coarse aggregate), conforming to IS 1489 Part I [26], IS 2386 Part III [27], and IS 383 [28], respectively, were used for this investigation. In addition to that, a commercially available “hooked-ends steel fibre” was added for preparing the fibre reinforced concrete (FRC). Table 1 gives steel fibre properties as provided by the maker. The casting and curing of the concrete proceeded with ordinary potable

Table 1. Properties of rigid fibre

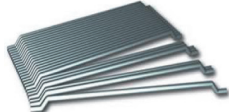
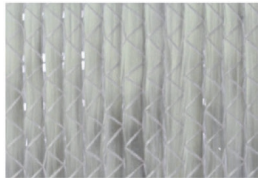
Properties	Length	Diameter	Aspect ratio	Tensile strength	Young’s modulus	Architecture
Steel fibre	30 mm	0.5 mm	60	532 MPa	210 GPa	

Table 2. Details of glass fabric

Technical		Construction		Architecture
Weave style	Unidirectional	0°	1200 g/m ² E-glass roving 2400 - 4800 tex	
		90°	50 g/m ² E-glass roving 300 tex	
Weight	1258 g/m ²	0°	8 g/m ² polyester 7.8 tex	
Yarn type	L1200 glass	width	1270 mm	

water. A commercially available, high-range water-reducer, i.e. Classic Superflo SP superplasticizer conforming to IS 9103 [29], was added. A commercially available ELO05 Unidirectional E-glass fabric was a strengthening agent considered in this study. ELO05 is a high-quality, unidirectional (where the fibres run predominantly in one planar direction) stitched glass fabric.

Technical and construction details of used unidirectional glass fabric provided by the makers are in Table 2. Selecting a resin type for bonding the FRP with the concrete surface is also a challenging task for the success of this method, since varieties of different epoxy resin additives with a wide range of mechanical properties are commercially available. Usually an additive contains two components: resin and hardener. Araldite LY 556 and Aradur HY 951 of epoxy resin and hardeners, respectively, were used in the study.

2.2. Testing of specimens and beams

A design mix M20 grade of concrete having a 1 : 2.01 : 3.36 mix ratio with 0.5 water-cement ratios was made according to IS 10262 [30]. The ratio was considered for cast control (concrete) specimens and beam specimens. The investigational study was steered on control specimens to find the properties of plain concrete and FRC, such as uniaxial compressive and Split-tensile strengths, according to IS 516 [31] and IS 5816 [32], respectively. For the casting of the specimen, cylinder-shaped moulds of size 150 x 300 mm, and 100 x 200 mm (viz. diameter x height) were used for determining the compressive and splitting tensile strengths, respectively. Following total fibre volume fractions (V_f) were maintained with a consistent increase of 0, 0.5, 1, and 1.5 %. Table 3 gives the test results of the various concrete specimens.

A total of nine beams of equal size were cast and tested for the experimental investigation, breadth 150 mm, depth 250 mm,

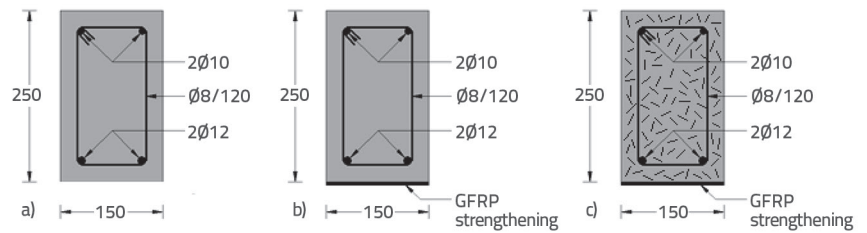


Figure 1. Beam details: a) Unstrengthened RC (control) beam; b) GFRP strengthened RC beams (RBL3 & RBL5); c) GFRP strengthened FRC beams (SF0.5L3, SF0.5L5, SF1.0L3, SF1.0L5, SF1.5L3 & SF1.5L5)

and length 3000 mm. One unstrengthened RC beam as “control beam”, one of each 3 and 5 mm thick GFRP strengthened RC beams, and three of each 3 and 5 mm thick GFRP strengthened RC beams mixed by three different volume fractions of steel fibres (i.e. 0.5 %, 1 %, and 1.5 %), were considered for the study. 2 Nos. of 12 mm diameter high yield steel deformed (HYSD) bars having yield strength = 415 MPa, as tensile reinforcement and 2 Nos. of 10 mm diameter HYSD hanger (secondary) bars in the compression zone, were used for all beams. 8 mm HYSD bars as shear reinforcement were equally spaced at 120 mm c/c throughout the span. Figure 1 shows schematic views of the reinforcement and strengthening of beams. The experimental beam details are given briefly in Table 3. A tilting-type drum mixer was used for preparation of green concrete. All the required measures were taken to avoid the formation of fibre balls and clustering while mixing the fibres. Figs 2.a and 2.b shows thoroughly mixing and pouring concrete in a mould. All the beams were cast in a batch. The beams were demoulded after 24 hours of casting and cured under water for 28 days before testing.

The strengthening performance of an externally bonded FRP laminated RC beam mainly depends on the types of adhesive resin used. According to the manufacturer’s instructions, epoxy resin (Araldite LY 556 & Hardener HY 951 mixing parts thru weight equal to 100:10) was prepared in a plastic bowl, and reinforcing fibres were cut as per beam size. The resin spread uniformly applied on the sternly prepared (i.e. on the tension)

Table 3. Properties of concrete and details of beams

Beam specimen	Concrete			Tensile steel rebar		Fibre volume fraction [%]	GFRP thick [mm]
	Compressive strength [MPa]	Tensile strength [MPa]	Young's modulus [GPa]	Number and diameter [mm]	Area [%]		
RB	26.70	3.80	25.83	2Ø12	0.60	0	0
RBL3	26.70	3.80	25.83	2Ø12	0.60	0	3
RBL5	26.70	3.80	25.83	2Ø12	0.60	0	5
SF0.5L3	27.50	4.20	26.19	2Ø12	0.60	0.5	3
SF0.5L5	27.50	4.20	26.19	2Ø12	0.60	0.5	5
SF1.0L3	29.05	5.55	26.98	2Ø12	0.60	1.0	3
SF1.0L5	29.05	5.55	26.98	2Ø12	0.60	1.0	5
SF1.5L3	32.25	7.60	28.37	2Ø12	0.60	1.5	3
SF1.5L5	32.25	7.60	28.37	2Ø12	0.60	1.5	5



Figure 2. Beam casting and strengthening in progress

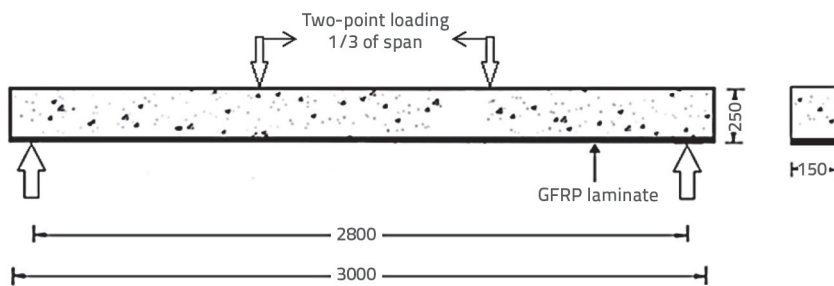


Figure 3. Test setup (all dimensions are in mm)

surface of concrete beams. Then the reinforcing glass fabric was gently placed and pressed into the uncured resin; at the same time, the surplus resin has squeezed out with a roller. The sufficient resin was applied to achieve full saturation of the fibres. Then the strengthened beams were tested after being cured at ambient temperature. Figures 2.c and 2.d shows the processes of beam strengthening. All the test variables are as given in Table 3.

Four-point bending instrumentation with a 500 kN loading capacity frame was used for testing the beams. Firstly, the beams were arranged with all test setups (i.e. the arrangement of the loading and measuring devices in the appropriate positions) in the frame. The loading was initiated and continued at the rate of 2.5 kN per increment monotonically until complete failure of the beams using a manually operated cylindrical hydraulic jack. Crack development and its propagation were monitored and measured during testing. A magnifying glass was gently used for monitoring and identifying a crack formation on the beam surface. A microscope was used exclusively for crack detection, having 0.02 mm least count used to measure the crack-widths

at a constant interval throughout the loading from first-crack formation to complete failure of the beams. Figure 3 shows a schematic diagram of the test setup. And Figure 4 shows a photographic view of the crack detection process.



Figure 4. Crack-width measurement in progress

3. Discussion

3.1. Crack characteristics

The development and propagation of cracks were observed and recorded throughout the testing process of laminated FRC beams. Very few flexural cracks initially formed in the tensile zone under the loading points after several increments of the load on the beams. Further increased load formation of cracks also increased towards mid-span and in shear-span. On further increases, the cracks propagated towards the compression zone and widened as well until the failure of the beams. Meanwhile, a crack detecting microscope bearing, a least count of 0.02 mm, was used to measure the crack-width (W_c) at regular intervals during the testing of beams right from an apparent first crack to the ultimate stage. The crack-width measurements were taken for all the beams at the level of tensile steel reinforcement and the constant moment region. The measured crack-widths at various (first crack, yield stage, and ultimate failure) stages of all the beams are in Table 4. Table 5 presents the details of the failures of the beams.

3.2. Crack-widths at various stages

The crack-widths corresponding to the first-crack, yield, and ultimate (complete) failure stages of the various beams are in Table 4. Figures 5 and 6 show the load versus crack-width response of all the tested beams. Discussions based on the above stages and the salient inferences on crack-width with

Table 4. Crack-widths of laminated FRC beams at various stages

Beam ID	Crack-width [mm]		
	First-crack stage	Yield stage	Ultimate stage
RB	0.07	0.44	0.58
RBL3	0.06	0.32	0.54
RBL5	0.05	0.30	0.52
SF0.5L3	0.05	0.28	0.46
SF0.5L5	0.04	0.25	0.42
SF1.0L3	0.04	0.20	0.42
SF1.0L5	0.03	0.18	0.38
SF1.5L3	0.03	0.17	0.38
SF1.5L5	0.02	0.16	0.32

respect to the lamination thickness versus total fibre volume (V_f) are given below.

3.2.1. First-crack stage

The crack-width of GFRP Strengthened RC beams (RBL3 & RBL5) was reduced slightly with increases in GFRP thickness over the control beam (RB). Further, the above reduction was higher for the highest thickness of laminate used (5 mm in the present study). Reduction in the above crack-width is 14.3 % and 28.6 % for 3 mm and 5 mm thick laminates compared to the control beam. Further, as the thickness of the laminate increased to 5 mm from 3 mm, there was a reduction of 16.7 % in the crack-width, indicating the influence of the laminate thickness on crack-width. In the above case, the reduction in crack-width is considered significant. The crack-width of the GFRP strengthened FRC beam appeared to be lowest at the highest fibre volume ($V_f = 1.5\%$), and the maximum thickness of GFRP (5 mm) was considered in the study.

Crack-widths of 5 mm GFRP strengthened FRC beams (SF0.5L5, SF1.0L5, & SF1.5L5) are reducing compared to the control beam, and the reductions are 42.9%, 57.1%, and 71.4% for respective 0.5, 1, and 1.5 percentage of fibre contents (V_f). It shows a combined effect of "fibres and lamination" in reducing the crack-width of strengthened FRC beams, which is highly advantageous in the durability aspect of a structural element and hence a structure. The reduction in crack-width is very high and continues to increase with an increase in V_f . Comparing the crack-widths of 5 mm strengthened FRC beams with that of the 5 mm strengthened RC beam (RBL5), the crack-width reduction in the former beams are 20%, 40%, and 60%, for $V_f = 0.5\%$, 1.0%, and 1.5%, respectively. In other words, for every 0.5% increase in V_f , there is a reduction of 20% in the crack-width of the strengthened FRC beams over the GFRP strengthening RC beam. It implies that the 3D hooked-end steel fibres played a vital role in controlling the crack-width even at the lowest fibre content (= 0.5%), and the above mentioned phenomenon continues to increase with the increase in fibre content.

3.2.2. Yield stage

The trend with respect to the reduction in crack-width of the GFRP strengthened FRC beams over the control beam at the yield stage is like in the first-crack stage. The crack-width for the 5 mm thick laminate at the yield stage for the range of V_f considered is minimum, like the first-crack stage. The maximum drop in the above mentioned crack-widths of strengthened RC beams (RBL3 & RBL5) over the control beam is 27.3% and 31.8% for 3 mm and 5 mm thick laminates. It seems that the role of laminate is high in reducing the crack-width at the yield stage. Further, as the laminate thickness increased to 5 mm instead of 3 mm, a reduction of 6.3% was observed in the crack-width. However, the effect of the above mentioned reduction in the crack-width is insignificant. The phenomenon indicates the role of laminate and its thickness on the crack-width.

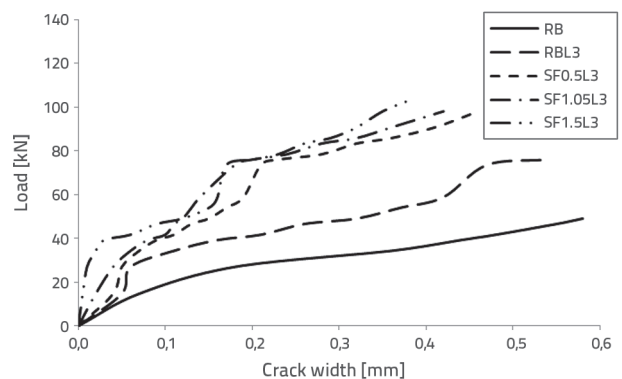


Figure 5. Load vs. crack-width for 3 mm GFRP strengthened FRC beams

While comparing the crack-widths of 5 mm strengthened FRC beams with the control beam, the former beams yield a reduction in crack-width of about 43.2%, 59.1%, and 63.6% for 0.5, 1.0 and 1.5% of fibre contents, respectively. It shows a combined effect of the "fibres and lamination" on reducing

the crack-width of GFRP strengthened FRC beams, which is very advantageous from the durability aspect of the structural element and hence the structure. Further, the reduction in crack-width is very high and continues to increase with an increase in V_f .

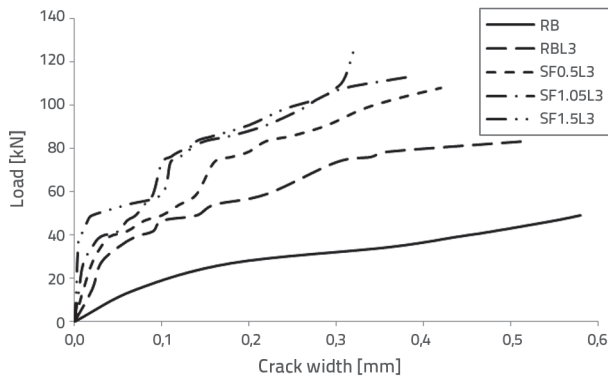


Figure 6. Load vs. crack-width for 5 mm GFRP strengthened FRC beams

Comparing the crack-widths of 5 mm strengthened FRC beams with 5 mm strengthened RC beams, the former beams have a reduction of crack-width of about 16.7 %, 40 %, and 46.7 % for 0.5, 1, and 1.5 % of fibre contents, respectively. It implies that the used steel fibres played a vital role in controlling the crack-width at the yield stage, even at the lowest fibre content, and the phenomenon continues to increase with the increase in fibre content. When comparing the role played by the steel fibres with the combined effect, the steel fibres influence the crack-width of strengthened FRC beams at the yield stage significantly.

3.2.3. Ultimate stage

The trend with respect to the decrease in crack-width at the ultimate stage of strengthened FRC beams over the control beam also seems to be like the first-crack and yield stages. The ultimate crack-width is lower for the highest (5 mm) laminate thickness used for the range of V_f considered is similar to that of the first-crack and yield stages. The decrease of ultimate crack-width of strengthened RC beams over the control beam is 6.9 % and 10.3 % for 3 and 5 mm thick laminates, which are insignificant. The trend of the role of laminate in respect of control of crack-width at the ultimate stage is opposite to that of the yield stage (i.e., the lamination played a relatively higher role up to the yield stage). As the thickness of the laminate increased to 5 mm from 3 mm thick, there was a reduction in the above crack-widths of about 3.4 %, which was also negligible. However, the above mentioned effect on crack-width at the ultimate stage due to the increase of thickness shows the same trend as discussed in the yield stage.

When comparing the crack-widths of 5 mm strengthened FRC beams with the control beam, the crack-widths reduced in the former beams are 27.6 %, 34.5 %, and 44.8 % for $V_f = 0.5$ %, 1.0

%, and 1.5 %, respectively. It seems that the above mentioned reduction in crack-widths is relatively less in the ultimate stage than at the yield stage. It indicates that the combined effect of the "fibres and lamination" in reducing the crack-width of GFRP strengthened FRC beams, which is very advantageous from the durability aspect of the structural element and hence the structure. Comparing the crack-widths of 5 mm strengthened FRC beams with that of the 5 mm strengthened RC beam, the former beams have a reduction in crack-width of about 19.2 %, 27 %, and 38.5 %, for $V_f = 0.5$ %, 1.0 %, and 1.5 %, respectively, which are relatively less in the ultimate stage than at yield stage. It reveals the role of steel fibres that significantly influence the crack-width even at the lowest fibre content and tends to increase when increasing the fibre content to the maximum at the highest fibre content used in this study. When comparing the above mentioned role of steel fibres with the combined effect, it seems that role of the fibre is relatively high in influencing the crack-widths of GFRP strengthened FRC beams.

3.3. Failure details

The failure details captured from the experimental investigation, such as the number of cracks, average crack spacing, and failure mode of strengthened FRC beams, are given in Table 5.

3.3.1. Crack formation

Numerous closely scattered flexural cracks were observed at the end of the testing on the surface of the laminated FRC beams. Discussion and salient inferences on the number of crack formation with respect to lamination thickness versus fibre volume (%) are as follow.

Crack formation varies with an increase in the thickness of laminate and V_f on FRC beams, and it is maximum for the higher lamination (5 mm) for the range of V_f considered. The crack formation increases with an increase in lamination thickness. The maximum increase in crack formation for 3 and 5 mm thick strengthened RC beams is 41.2 % and 66.7 % compared to the control beam. It shows a significant increase in crack formation on both laminates, which may be due to the stiffening effect of laminates. While comparing the 5 mm thick strengthened FRC beams with the control beam, the maximum increase in the crack formation is 91.7 % for $V_f = 1.5$ %. Similarly, comparing the 5 mm thick strengthened FRC beams and the 5 mm thick strengthened RC beam, the maximum increase in the crack formation is 15 %, corresponding to $V_f = 1.5$ %. The above comparisons show a combined effect on strengthened FRC beams that influences the formation of cracks.

3.3.2. Average crack spacing

During the experimental investigation, crack formations and their propagation were monitored and recorded consistently. In general, flexural cracks developed primarily at the region

Table 5. Failure details of various tested beams

Beam ID	No. of visible crack	Average crack spacing [mm]	Mode of failure
RB	12	156.20	Yielding of tensile rebar yielding followed by crushing of concrete at compression zone
RBL3	17	95.60	Widening of flexural cracks at concrete-GFRP bonding interface followed by debonding
RBL5	20	81.00	Widening of flexural cracks at concrete-GFRP bonding interface followed by debonding
SF0.5L3	18	89.30	Widening of flexural cracks at concrete-GFRP bonding interface followed by debonding
SF0.5L5	20	76.20	Widening of flexural cracks at concrete-GFRP bonding interface followed by debonding
SF1.0L3	21	85.40	Widening of flexural cracks followed by GFRP rupture with bursting sound
SF1.0L5	22	72.40	Widening of flexural cracks at concrete-GFRP bonding interface followed by debonding
SF1.5L3	23	80.20	Widening of flexural cracks at concrete-GFRP bonding interface followed by debonding
SF1.5L5	23	67.10	Widening of flexural cracks at concrete-GFRP bonding interface followed by debonding

of constant-moment and then some flexural-shear (diagonal) cracks also developed in the shear-span of the beams. The discussion and salient inferences on the average crack spacing (see Table 5) with respect to the laminate thickness versus total fibre content (V_f) are as follows under.

The average crack spacing of FRC beams decreases with an increase in the lamination and V_f used in this study. Further, there is a change in the failure mode to ductile from brittle. The crack spacing is minimum for the higher thickness of the laminate, for the range of V_f considered. The crack spacing decreases with an increase in lamination thickness. The maximum decrease in the crack spacing on strengthened RC beams is 38.8 % and 48.1 % for 3 and 5 mm laminated beams, respectively, over the control beam. And it can be seen that the above decrease is significant for 3 and 5 mm laminated beams, which may be due to the stiffening effect of laminates. However, a reduction in the crack spacing found was the maximum of 57 % for the 5 mm laminated FRC beam corresponding to $V_f = 1.5$ % compared to that of the control beam. Similarly, the decrease in the crack spacing found maximum corresponding to $V_f = 1.5$ % is 17.2 % for the 5 mm laminated FRC beam, compared to the 5 mm laminated RC beam. The above mentioned comparisons show a "combined effect" on the strengthened FRC beams that influence the crack spacing.

3.3.3. Mode of failure

Failure details of the various beams are in Table 5. Three different failure types were observed from the experimental study: concrete crushing, debonding of laminate, and GFRP rupture. The control beam (RB) failed in concrete crushing at the compression zone following tensile steel yielding. Strengthened RC beams (RBL3 and RBL5) and strengthened FRC beams (SF0.5L3, SF0.5L5, SF1.0L5, SF1.5L3, and SF1.5L5) failed in laminate debonding. The laminated FRC beam (SF1.0L3) failed in GFRP rupture with a bursting sound. The above failure modes generally fall under flexural failure, and none of the laminated beams exhibited premature failure by delamination. Failure of the various tested beams is shown in Figure 7.

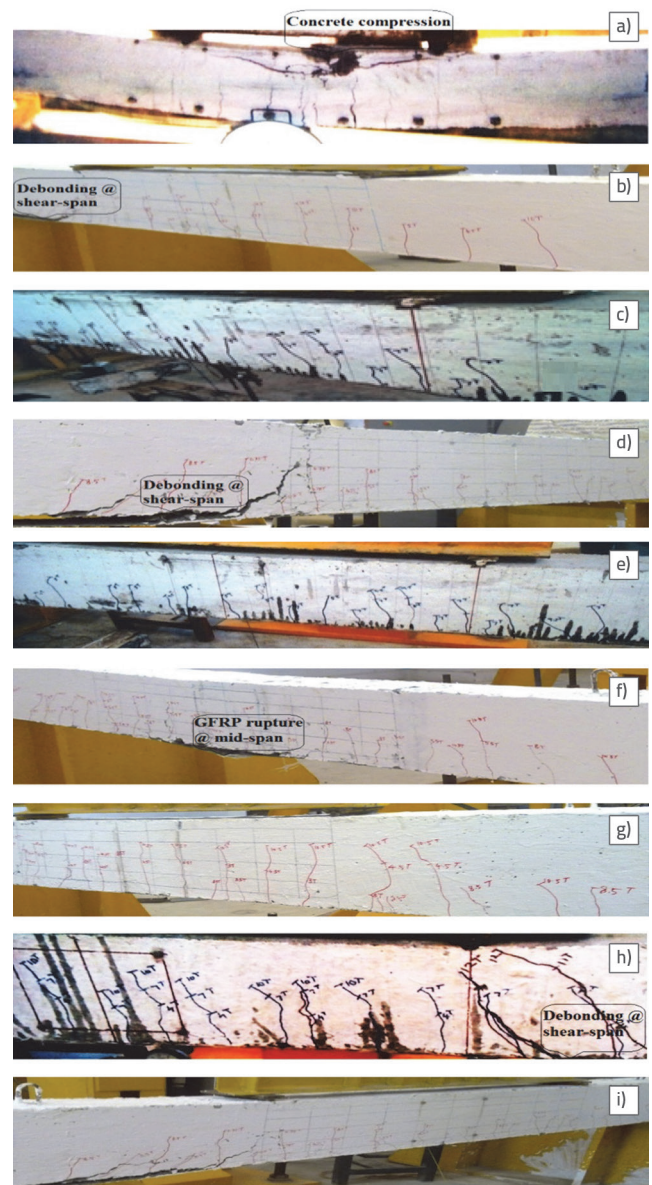


Figure 7. Failure mode and crack pattern of various beams: a) RB; b) RBL3; c) RBL5; d) SF0.5L3; e) SF0.5L5; f) SF1.0L3; g) SF1.0L5; h) SF1.5L3; i) SF1.5L5

3.4. Numerical comparison

Numerical methods to Validate any Design have various advantages compared to the analytical and or experimental method(s), such as: (a) application even if a physical prototype is not available; (b) results achieved faster; (c) solving complex problems; (d) results achieved on entire geometry. But, the only disadvantage of the numerical methods is that the results extracted could be approximate. There have been four numerical methods, including the finite element analysis method (FEA), boundary element method, finite volume method, and finite difference method. Of the above, FEA based well-known ANSYS software [33] was used for modelling and comparing the experimental results. The numerical Design Validation has been processed for all the beams, exclusively on the concrete (tensile and compressive) stresses, load, displacement, and crack formation at different stages. The beams were modelled before by selecting appropriate in-built elements that meet the real-time material behaviour and were the boundary (support and loading) conditions simulated in accordance with the test setup. Figure 8 shows a meshed GFRP laminated full-scale ANSYS beam model.

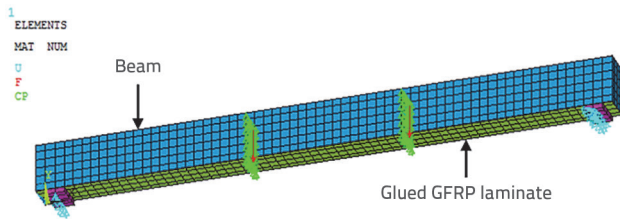


Figure 8. Meshed GFRP laminated beam model with boundary conditions

3.4.1. Concrete failure criteria in ANSYS

For general concrete modelling, the in-built RC SOLID65 element in the FEA software can model cracking and crushing (brittle) modes of failures. Eqn. (1) for concrete material model the cracking/crushing failure criterion because of the state of multiaxial stress if it is satisfied [33]:

$$\frac{F}{f_c} - S \geq 0 \tag{1}$$

To define the brittle surface failure of concrete in the model, constants f_t, f_c, f_{cb}, f_1 and f_2 are the strength (temperature dependent) parameters needed as input eqns. (2), (3), (4) along with f_t and f_c out of which the f_t and f_c need to be specified to define the failure surface as shown in Figure 9. It shows three failure surfaces as projections between the σ_{xp} and σ_{yp} planes where that of non-zero principal stresses in the respective directions of x and y, even though a failure mode is the function of σ_{zp} and the rest of the constants are default in [33]:

$$f_{cb} = 1,2 f_c \tag{2}$$

$$f_1 = 1,45 f_c \tag{3}$$

$$f_2 = 1,725 f_c \tag{4}$$

The 3-D failure surface in the principal stress space is shown in Figure 9. If the above condition is satisfied for stress states, then only the default values are valid. Hence at low hydrostatic stress component condition eqn. (5) applies to stressful situations. If an extensive hydrostatic stress component is anticipated, all failure parameters have to be specified.

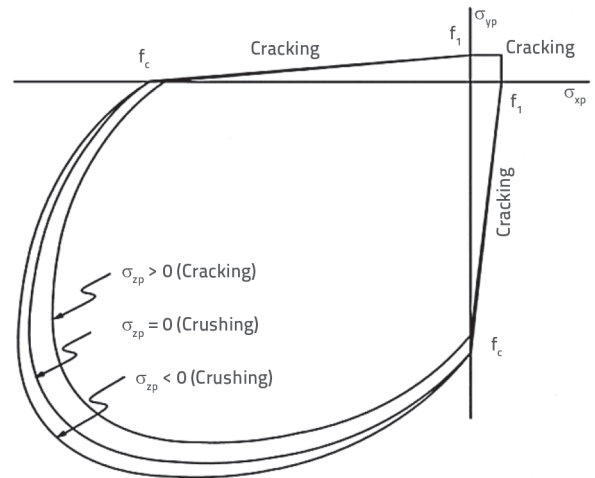


Figure 9. Failure surface in principal stress space with nearly biaxial stress

$$|\sigma_h| \leq \sqrt{3} f_c \tag{5}$$

$$\sigma_h = \text{hydrostatic stress state} = \frac{1}{3}(\sigma_{xp} + \sigma_{yp} + \sigma_{zp}) \tag{6}$$

Otherwise, if eqn. (5) is unsatisfied with the assumed default values, i.e. the eqns. (2) to (4) evaluate incorrect concrete strength. If the principal stress component is greater than the ultimate uniaxial tensile strength of concrete (f_t) and the concrete material model will crack provided f_c equals -1.0 to suppress the crushing capability of the concrete material. The functions F and S expressed in terms of principal stresses denoted as σ_1 (maximum), σ_2 (average), and σ_3 (minimum) and $\sigma_1 \geq \sigma_2 \geq \sigma_3$, where σ_1 and σ_3 can be considered by eqns. (7) and (8):

$$\sigma_1 = \max(\sigma_{xp}, \sigma_{yp}, \sigma_{zp}) \tag{7}$$

$$\sigma_3 = \min(\sigma_{xp}, \sigma_{yp}, \sigma_{zp}) \tag{8}$$

The concrete failure in SOLID65 element modelling categorized into four domains such as:

$$0 \geq \sigma_1 \geq \sigma_2 \geq \sigma_3 \text{ (compression – compression – compression)}$$

$$\sigma_1 \geq 0 \geq \sigma_2 \geq \sigma_3 \text{ (tensile – compression – compression)}$$

$$\sigma_1 \geq \sigma_2 \geq 0 \geq \sigma_3 \text{ (tensile – tensile – compression)}$$

$$\sigma_1 \geq \sigma_2 \geq \sigma_3 \geq 0 \text{ (tensile – tensile – tensile).}$$

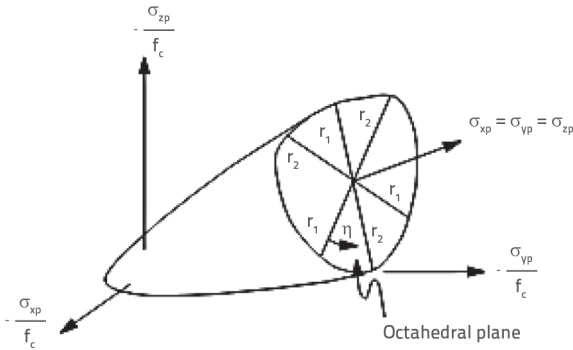


Figure 10. 3D failure surface in principal stress space

Figure 10 shows the failure surface in the principal stress space with nearly biaxial stress. The functions F and S describe independently in each domain. The above four functions describe the general function F and S , denoted as F_1, F_2, F_3, F_4 and $S_1, S_2, S_3,$ and S_4 , respectively. "The functions $S_i (i = 1,4)$ have the properties that the surface they describe is continuous while the surface gradients are not continuous when any of the principal stresses changes sign. For example, if σ_{xp} and σ_{yp} are both negative (compressive) and σ_{zp} is slightly positive (tensile), cracking would be predicted in a direction perpendicular to σ_{zp} . If σ_{zp} is zero or -ve slightly then, the material is assumed to crush" [33].

3.4.2. Principal stresses in concrete

At the integration points of the SOLID65 (concrete) elements, principal stresses and strains are predicted using the ANSYS postprocessor. A typical integration point in the concrete SOLID65 element is as in Figure 11. The contour plots of principal stresses (σ_1 and σ_3) from the nodal solution for the various beam models is as shown in Figure 12. First principal stress (σ_1) and third principal stress (σ_3) correspond to the maximum tensile and compressive stresses in the concrete, respectively. Noticeable is that the contour plot of σ_1 shows maximum tensile stress at the bottom face of the FEM. Moreover, the contour plot of the σ_3 shows a higher concentration of compressive stress at the top surface of the FEM.

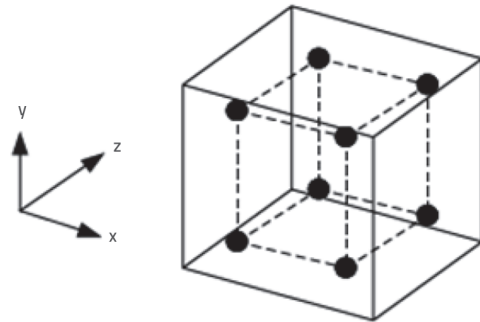


Figure 11. Integration points in SOLID65 element

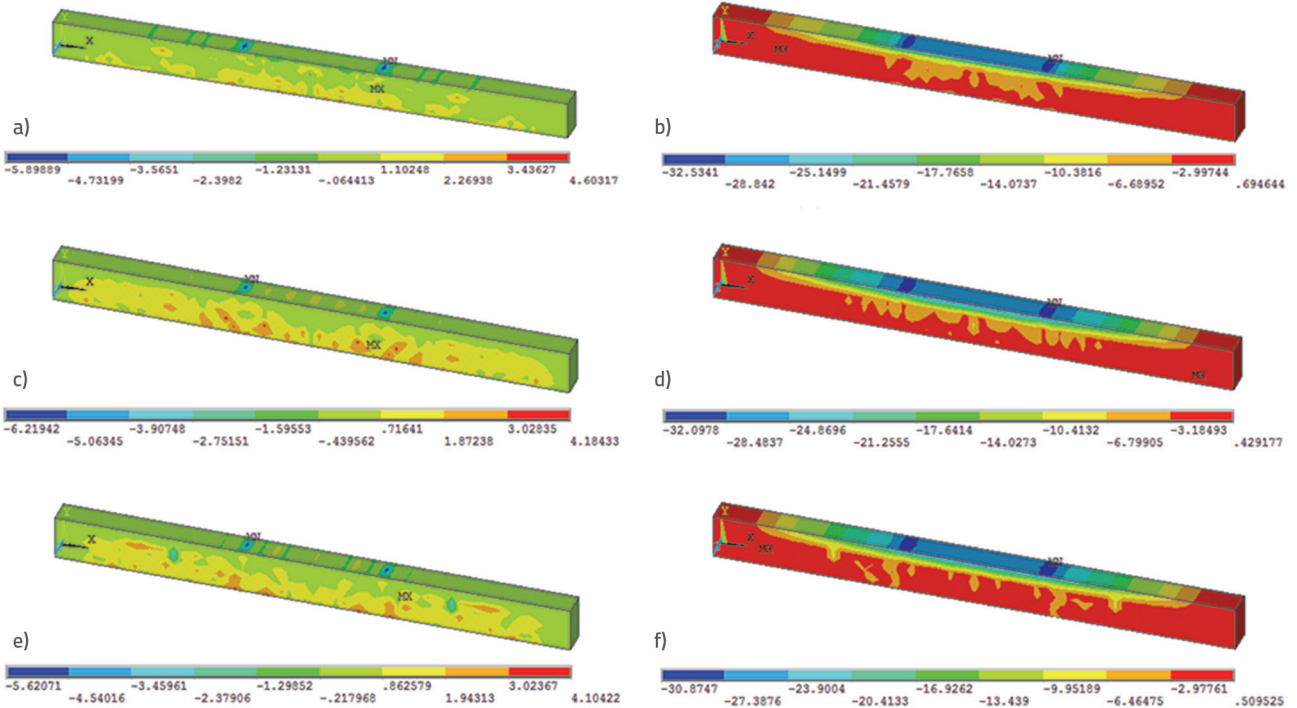


Figure 12. Stress distribution of various beam models: a) RB: First principal stress, σ_1 ; b) RB: Third principal stress, σ_3 ; c) RBL3: First principal stress, σ_1 ; d) RBL3: Third principal stress, σ_3 ; e) RBL5: First principal stress, σ_1 ; f) RBL5: Third principal stress, σ_3

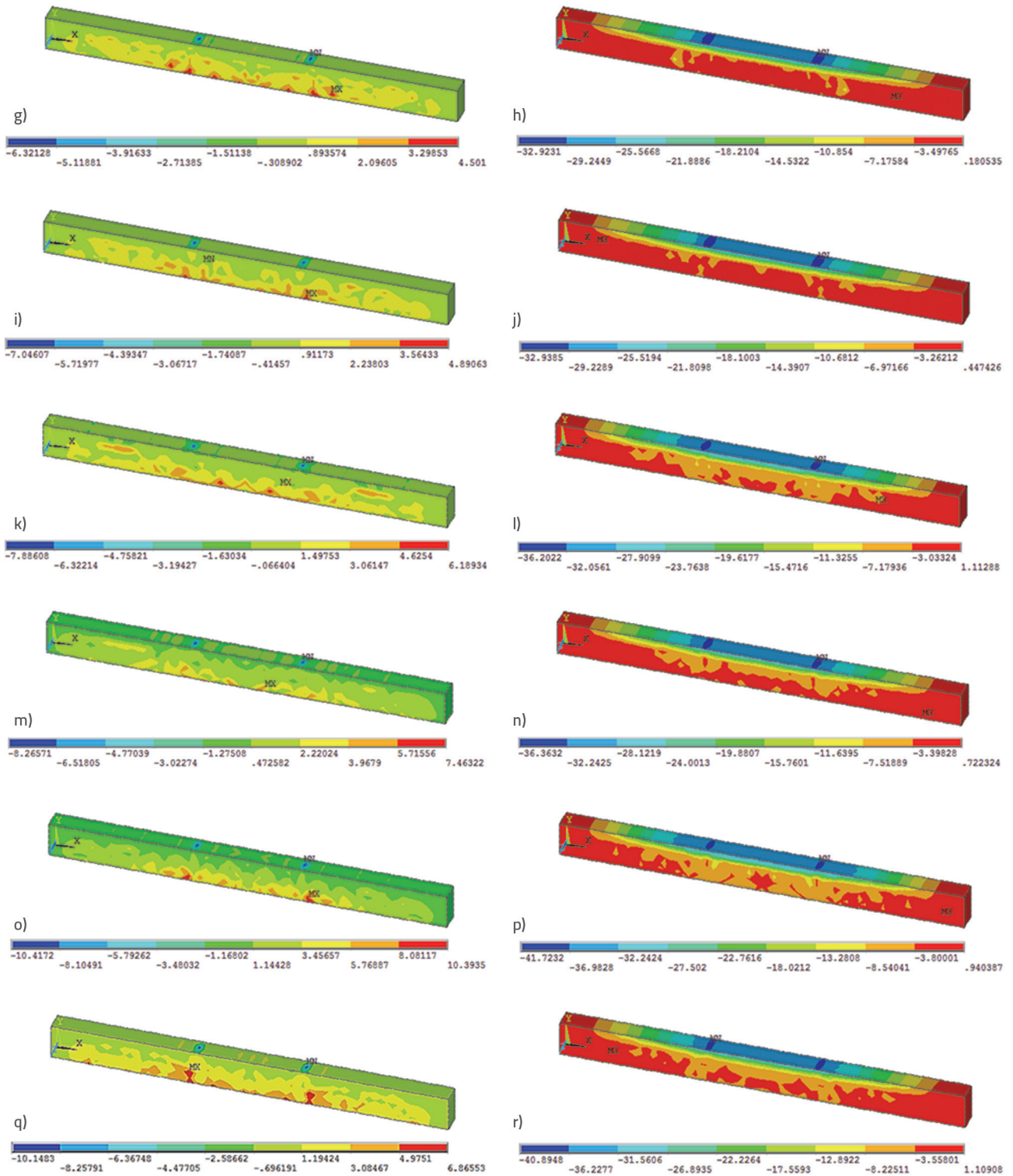


Figure 12. Stress distribution of various beam models: g) SF0.5L3: First principal stress, σ_1 ; h) SF0.5L3: Third principal stress, σ_3 ; i) SF0.5L5: First principal stress, σ_1 ; j) SF0.5L5: Third principal stress, σ_3 ; k) SF1.0L3: First principal stress, σ_1 ; l) SF1.0L3: Third principal stress, σ_3 ; m) SF1.0L5: First principal stress, σ_1 ; n) SF1.0L5: Third principal stress, σ_3 ; o) SF1.5L3: First principal stress, σ_1 ; p) SF1.5L3: Third principal stress, σ_3 ; q) SF1.5L5: First principal stress, σ_1 ; r) SF1.5L5: Third principal stress, σ_3

3.4.3. ANSYS crack symbol

Figure 13 shows the ANSYS concrete model cracking symbol like a circle exhibited perpendicular to the direction of the principal stress, while cracking shows when the tensile stress of the concrete increases beyond the ultimate tensile strength. Figure 14 shows a typical cracking circle in three different planes, formed at the integration points with three different colours (or stages) such as red, green, and blue, via the first, second, and third cracks, respectively. After reaching the third stage (i.e., multiple crack formations), the elements linked in the SOLID65 will be history, and the concrete material model exhibit softening behaviour in all directions. The three possible types of crack formations (one-half of beam RB shown in Figure 14), modelled by the ANSYS software, are briefed as under.

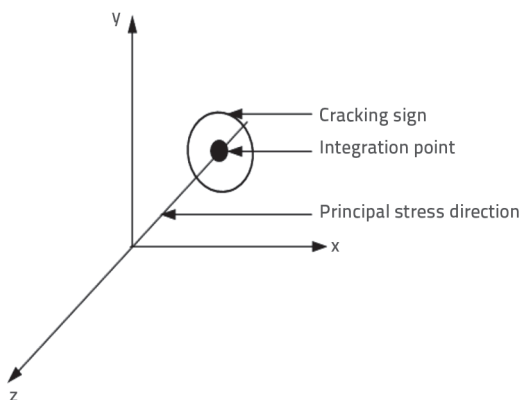


Figure 13. ANSYS cracking symbol

Flexural Cracks: When the principal tensile stresses occur along the length of the beam, this type of crack predominantly develops and propagates from the initiation of the first crack. The cracking sign of circles appears like vertical lines (Figure 14) along the length of the beam if the principal stresses go beyond the tensile strength of the concrete. These lines represented as

“flexural cracks” were formed at the point of integration of the SOLID65 elements.

Compressive Cracks: Generally, compressive type of cracking sign appears like a circle along the beam model under the load points at integration points in the concrete elements, as shown in Figure 13. Initially, the crack develops and propagates towards the direction of externally applied load (F) then because of Poisson's effect the tensile strains subsequently developed in the elements [33-34]. Similar behaviour is realized in this analysis since load applied on along width of the beam resulting to tensile strain developed on along depth of the beams. The crack appears like a circle (Figure 14) along the length of beams, denoted as a compressive crack.

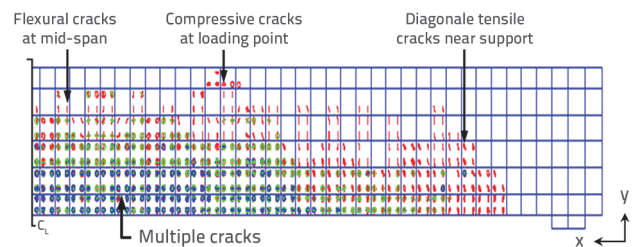


Figure 14. Typical cracking symbols in ANSYS beam model

Tensile Cracks: Generally, normal tensile stress develop along the length of the beams (i.e. in the x direction), and shear stress develops across the beams (i.e. in the xz plane). “Inclined line” of cracking signs are observed (see Figure 14) if tensile and shear stresses together acting on the concrete SOLID65 elements as a result of principal tensile stresses seems to be inclined if it exceeds the tensile strength of the concrete at the point of integration point of the SOLID65 elements. The inclined line of the cracking symbol is termed a diagonal tensile crack.

3.4.4. Element centroid crack pattern

In addition to the above mentioned types of cracks, the ANSYS also predicts three different cracking natures simultaneously

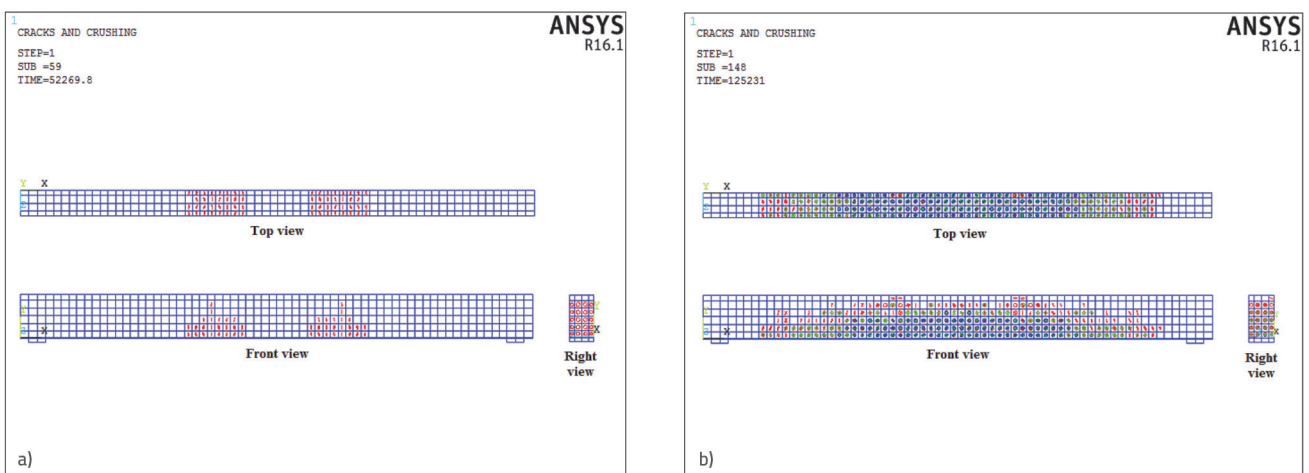


Figure 15. Element centroid crack patterns of SF1.5L5 beam model at various stages; a) First-crack stage; b) Ultimate stage

on each substep right from the formation of first-crack to the ultimate failure stage, as is represented by three different colours: red, green, and blue (Figure 14). The red, green, and blue indicate first crack, second crack, and third crack, respectively. Discussion and salient inferences based on the above are as follows.

It seems that the "first-crack" of all the beam models formed below the points of the loading area at the tension zone of the beam. The above behaviour was also visually experienced during testing. In the subsequent substeps, the "flexural cracks" are developed further towards the mid-span and shear span of the beam models. The crack length is also propagated towards the compression zone of the beams. The above development and propagation of cracks are similar to the observations made during experimental investigations. A few "compressive cracks" and "diagonal tensile cracks", were formed near the loading points and in the shear span, respectively, in the beam at the ultimate stage. Further, the maximum number of multiple flexural cracks also formed in the mid-span. The above trend is similar to the observations made during experimental investigations.

The predicted crack formation and its propagation of the SF1.5L5 beam at the first-crack stage and the ultimate stage are shown in Figure 15. It shows multiple cracks in the extreme tension fibre of the beam at the ultimate stage indeed that there may be a possibility of concrete cover separation or debonding of laminate from the concrete surface, due to the excessive concentration of flexural cracks at the extreme tension face of the beam.

3.5. Codal comparison

In view of the structural safety and serviceability requirement, the IS 456 clause 35.3.2 [35] recommends that the surface crack-width should not generally exceed 0.3 mm. From the above perspective, the experimentally obtained crack-width of all the GFRP strengthened FRC beams at the yield stage is well within the recommended value. Moreover, the maximum crack-width of the beam SF1.5L5, even at the ultimate stage, shows close adherence to the codal provision (Table 4).

4. Conclusion

The following salient conclusions are drawn based on the results and the salient inferences of the experimental and numerical investigations on GFRP strengthened hooked-end steel fibre reinforced concrete (FRC) beams:

- The crack-width of the GFRP strengthened RC beams reduces with increases in the laminate thickness over the unstrengthened RC (control) beam. The maximum decrease in crack-width of the strengthened RC beams over the control beam (without GFRP strengthening) at the first-crack load is about 14 % and 29 %, and at the yield load it is about 27 % and 32 % for 3 and 5 mm thick laminates, respectively. However, at the ultimate stage, the maximum reduction is only about 7 % and 10 % for 3 mm and 5 mm, respectively, over the control beam. It shows that the role played by lamination up to the yield stage is high with respect to crack-width. The reduction in crack-widths of 5 mm laminated

FRC beams" at $V_f = 1.5$ % over the control beam is about 71 %, 63 %, and 44 %. It shows a "combined effect" in reducing the crack-width of laminated FRC beams. The above mentioned effect is consistently significant and very high in all the stages. This phenomenon is highly advantageous from the ductility aspect of a structural element and hence the structure.

- Three typical failure modes experienced in this study include crushing of concrete, debonding of laminates, and rupture of laminate. The control beam fails in concrete crushing at the compression zone preceded by tensile steel yielding, whereas in the GFRP strengthened FRP beams, rupture and or debonding failures were the typical failure modes observed as stated in the literature, conforming to the common and the characterized failure modes.
- In the context of experimental results with the numerical design validation, the FEA-based software has the capability to predict the formation of cracks at different stages of the RC beam models. The predictions of the crack formation and propagation at the various stages and crack types in the RC beam models explicitly agreed well with the experiment.
- The holistic behaviour of externally FRP strengthened RC beams mixed by the 3D hooked-end steel fibres gives a realistic and viable method in the context of structural strengthening. However, further studies are needed in the aspect of the long-term performance of GFRP strengthened hooked-end steel fibre reinforced concrete beams for the betterment of the strengthening method.

Nomenclature

- 3D - Three dimensional
- F - function of the principal stress state ($\sigma_{xp}, \sigma_{yp}, \sigma_{zp}$)
- V_f - Total fibre volume fraction
- f_1 - ultimate compressive strength for a state of biaxial compression superimposed on hydrostatic stress state
- f_2 - ultimate compressive strength for a state of uniaxial compression superimposed on hydrostatic stress state
- f_c - ultimate uniaxial compressive/crushing strength of concrete
- f_{cb} - ultimate biaxial compressive strength of concrete
- f_t - ultimate uniaxial tensile strength of concrete
- s - failure surface expressed in terms of principal stresses and five input parameters $f_t, f_c, f_{cb}, f_1, f_2$
- σ_h^a - ambient hydrostatic stress state
- $\sigma_1, \sigma_2, \sigma_3$ - maximum, average, and minimum, principal stresses respectively
- $\sigma_{xp}, \sigma_{yp}, \sigma_{zp}$ - principal stresses in principal directions x, y, z, respectively

Acknowledgements

This forms a part of the research work of the author. The facilities provided and the cooperation extended for first conducting this research work in the Department of Civil Engineering, Pondicherry Engineering College, Pondicherry, India, are gratefully acknowledged.

REFERENCES

- [1] Tarafder, N., Swain, R.: Durability and case study of fiber reinforced polymer (Frp), *IOSR Journal of Mechanical and Civil Engineering*, 13 (2016) 6, pp. 53-62, <https://doi.org/10.9790/1684-1306035362>
- [2] Amrana, Y.H.M., Alyousef, R., Rashid, R.S.M., Alabduljabbar, H., Hung, C.C.: Properties and applications of FRP in strengthening RC structures: A review, *Structures*, 16 (2018), pp. 208-238, <https://doi.org/10.1016/j.istruc.2018.09.008>
- [3] Ibrahim, S.S., Eswari, S., Sundararajan, T.: Behaviour of hybrid fibre reinforced concrete beams strengthened with GFRP laminates, *Structural Engineering and Mechanics*, 66 (2018), pp. 631-636, <https://doi.org/10.12989/sem.2018.66.5.631>
- [4] Abbood, I.S., Odaa, S.A., Hasan, K.F., Jasim, M.A.: Properties evaluation of fiber reinforced polymers and their constituent materials used in structures – A review, *Materials Today: Proceedings*, 43 (2021), pp.1003-1008, <https://doi.org/10.1016/j.matpr.2020.07.636>
- [5] Cvetanovska, G.N., Roshi, A., Bojadjeva, J., Bojadjiev, J., Trajcevski, Z.: Quasi-static tests on RC building columns strengthened with CFRP, *GRAĐEVINAR*, 73 (2021) 8, pp. 805-818, <https://doi.org/10.14256/JCE.3087.2020>
- [6] Cvetanovska, G.N., Roshi, A., Bojadjiev, J., Bojadjeva, J., Trajcevski, Z.: Performance of CFRP-confined concrete cylinder specimens - laboratory study, *GRAĐEVINAR*, 74 (2022) 2, pp. 95-104, <https://doi.org/10.14256/JCE.3020.2020>
- [7] Vivekanandan, R., Karmegam, A.: Failure analysis of hybrid strengthened RC square column, *GRAĐEVINAR*, 76 (2024) 1, pp. 25-34, <https://doi.org/10.14256/JCE.3837.2023>
- [8] Aravind, N., Samanta, A.K., Roy, D.K.S., Thanikal, J.V.: Retrofitting of reinforced concrete beams using fibre reinforced polymer (FRP) composites – A review, *Journal of Urban and Environmental Engineering*, 7 (2013), pp.164-175, <https://doi.org/10.4090/juee.2013.v7n1.164175>
- [9] Abid, A.L.: Critical review of strength and durability of concrete beams externally bonded with FRP, *Cogent Engineering*, 5 (2018), 1-27, <https://doi.org/10.1080/23311916.2018.1525015>
- [10] Siddika, A., Al-Mamun, M.A., Alyousef, R., Amran, Y.H.M.: Strengthening of reinforced concrete beams by using fiber-reinforced polymer composites: A review, *Journal of Building Engineering*, 25 (2019), 100798, <https://doi.org/10.1016/j.jobbe.2019.100798>
- [11] Demir, A., Ince, Y., Altok, T.Y.: Experimental and numerical investigation of RC beams strengthened with CFRP composites, *GRAĐEVINAR*, 73 (2021) 6, pp. 605-616, <https://doi.org/10.14256/JCE.3051.2020>
- [12] Kang, T.H.K., Howell, J., Kim, S., Lee, D.J.: A state-of-the-art review on debonding failures of FRP laminates externally adhered to concrete, *International Journal of Concrete Structures and Materials*, 6 (2012), pp. 123-134, <https://doi.org/10.1007/s40069-012-0012-1>
- [13] Danraka, M.N., Mahmud, H.M., Oluwatosin, O.J.: Strengthening of reinforced concrete beams using FRP technique: A review, *International Journal of Engineering Science and Computing*, 7 (2017) 6, pp. 13199-13213.
- [14] Ibrahim, S.S., Kandasamy, S., Subashchandrabose, R., Baskar, S., Madhava, V.: Performance enhancement of externally bonded reinforced concrete beams with 3D hooked-end steel fibres". *Case Studies in Construction Materials*, 17 (2022), pp01181, <https://doi.org/10.1016/j.cscm.2022.e01181>
- [15] Wypych, G.: *Mechanisms of Adhesion Loss*, Handbook of Adhesion Promoters, Elsevier B.V., 2018.
- [16] Zhang, Z., Xiao, Y., Zhuge, P., Zhang, X.: Experimental investigation on the interfacial debonding between FRP sheet and concrete under medium strain rate, *Hindawi International Journal of Polymer Science*, (2019), pp. 1973453, <https://doi.org/10.1155/2019/1973453>
- [17] Al-Saawania, A.M., El-Sayed, K.A., Al-Negheimish, I.A.: Assessment of plate-end debonding design provisions for RC beams strengthened with FRP, *Latin American Journal of Solids and Structures*, 17 (2020) 2, e255 1/18, <https://doi.org/http://dx.doi.org/10.1590/1679-78255920>
- [18] Gribniak, V., Tamulenas, V., Ng, P.N., Arnautov, A.K., Gudonis, E., Misiunaite, I.: Mechanical behavior of steel fiber-reinforced concrete beams bonded with external carbon fiber sheets, *Materials*, 10 (2017), pp. 1-18, <https://doi.org/10.3390/ma10060666>
- [19] Abbass, A., Abid, S., Ozakça, M.: Experimental investigation on the effect of steel fibers on the flexural behavior and ductility of high-strength concrete hollow beams, *Advances in Civil Engineering*, 2019 (2019), pp. 1-13, <https://doi.org/10.1155/2019/8390345>
- [20] Markić, T., Amin, A., Kaufmann, W., Pfyl, T.: Strength and deformation capacity of tension and flexural RC members containing steel fibers, *Journal of Structural Engineering*, 146 (2020), [https://doi.org/10.1061/\(ASCE\)ST.1943-541X.0002614](https://doi.org/10.1061/(ASCE)ST.1943-541X.0002614)
- [21] Sharaky, I.A., Eldin, H.K.S., Shehata, M.M., Mohamed, H.: Flexural response of RC beams cast with normal and steel fibre concrete internally reinforced with various types of FRP bars, *GRAĐEVINAR*, 72 (2020) 12, pp. 1117-1130, <https://doi.org/10.14256/JCE.3009.2020>
- [22] Gribniak, V., Arnautov, A.K., Norkus, A., Tamulenas, V., Gudonis, E., Sokolov, A.: Experimental investigation of the capacity of steel fibers to ensure the structural integrity of reinforced concrete specimens coated with CFRP sheets, *Mechanics of Composite Materials*, 52 (2016), pp. 401-410, <https://doi.org/10.1007/s11029-016-9592-1>
- [23] Ali, A., Iqbal, S., Holschemacher, K., Bier, T.A.: Comparison of flexural performance of lightweight fibre reinforced concrete and normal weight fibre reinforced concrete, *Periodica Polytechnica Civil Engineering*, 61 (2017), pp. 498-504, <https://doi.org/10.3311/PPci.8858>
- [24] Mohajerani, A., Hui, S.Q., Mirzababaei, M., Arulrajah, A., Horpibulsuk, S., Kadir, A.A., Rahman, M.T., Maghool, F.: Amazing types, properties, and applications of fibres in construction materials, *Materials*, 12 (2019), pp.1-45, <https://doi.org/10.3390/ma12162513>
- [25] Kytinou, V.K., Chalioris, C.E., Karayannis, C.G., Elenas, A.: Effect of steel fibers on the hysteretic performance of concrete beams with steel reinforcement-tests and analysis, *Materials*, 13 (2020), pp. 1-32, <https://doi.org/10.3390/ma13132923>
- [26] IS 1489-Part I: Specification for Portland Pozzolana Cement, Part 1: Flyash Based, New Delhi, India, 1991.
- [27] IS 2386-Part III: Methods of Test for Aggregates for Concrete, Part 3: Specific Gravity, Density, Voids, Absorption and Bulking, New Delhi, India 1963.
- [28] IS 383: Specification for Coarse and Fine Aggregates from Natural Sources for Concrete, New Delhi, India, 1970.
- [29] IS 9103: Specification for Concrete Admixtures, New Delhi, India, 1999.
- [30] IS 10262: Concrete Mix Proportioning, New Delhi, India, 2009.
- [31] IS 516: Methods of Tests for Strength of Concrete, New Delhi, India, 1959.
- [32] IS 5816: Method of Test Splitting Tensile Strength of Concrete, New Delhi, India, 1999.
- [33] SAS: Finite Element Analysis System, ANSYS Release 16.1, © SAS IP, Inc., 2015.
- [34] Dahmani, L., Khennane, A., Kaci, S.: Crack identification in reinforced concrete beams using ANSYS software, *Strength of Materials*, 42 (2010) 2, pp. 232- 240.
- [35] IS 456: Plain and Reinforced Concrete - Code of Practice [CED 2: Cement and Concrete], New Delhi, India, 2000.